Fluid Phase Equilibria 277 (2009) 131–144

Contents lists available at ScienceDirect

Fluid Phase Equilibria

journal homepage: www.elsevier.com/locate/fluid

Developing a predictive group-contribution-based SAFT-VR equation of state

Yun Peng, Kimberly D. Goff, M. Carolina dos Ramos, Clare McCabe*

Department of Chemical and Biomolecular Engineering, Vanderbilt University, Nashville, TN 37215-1604, United States

ARTICLE INFO

Article history:
Received 22 August 2008
Received in revised form
10 November 2008
Accepted 10 November 2008
Available online 19 November 2008

Keywords:
Phase equilibria
Pure fluids
Mixtures
Group contribution
Heteronuclear
SAFT
GC-SAFT-VR

ABSTRACT

The hetero-segmented version of the statistical associating fluid theory for potentials of variable range (hetero-SAFT-VR) is used to develop a predictive molecular-based group-contribution SAFT-VR equation of state (GC-SAFT-VR). The hetero-SAFT-VR approach models molecules composed of segments of different size and/or energies of interaction enabling an accurate description of real molecules composed of different functional groups. The differences in interactions between functional groups are maintained throughout the theory in contrast to other approaches in which the parameters for functional groups are averaged in order to model a molecule as a homonuclear chain with "group-averaged" parameters. Through the GC-SAFT-VR approach we can study the effect of molecular functionality and topology on the thermodynamic properties of real fluid systems, since parameters are determined for each functional group and chain connectivity is explicitly specified. In this initial study GC-SAFT-VR parameters are developed for key organic functional groups (CH_3, CH_2, CH_2=CH, C=O, C_6H_5, OCH_3 and OCH_2) by fitting to experimental vapor pressure and saturated liquid density data for a selected group of compounds that contain these functional groups. The transferability of the parameters obtained is tested by comparing theoretical predictions with experimental data for pure fluids not included in the fitting process and binary mixtures. Using the GC-SAFT-VR approach good agreement is obtained between experimental data and the theoretical predictions for pure substances, including isomers, and their mixtures. The GC-SAFT-VR approach is able to accurately predict the effect of molecular functionality on mixture phase behavior without fitting to any experimental data for the system being studied.

1. Introduction

The study of fluid phase behavior and the development of accurate theoretical approaches to predict physical properties and phase diagrams remains an enduring challenge and an area of great fundamental and applied significance. Reliable methods for the theoretical prediction of thermophysical properties and phase equilibria are essential to the chemical, biochemical and energy industries, and are made all the more critical as energy costs require more frequent re-analysis of existing chemical process [1] as well as the design of new novel energy efficient processes.

While the goals of fluid property prediction have not changed – i.e., understanding and accurately modeling their thermodynamics and phase behavior – the systems of interest are of increasing complexity, such as heavy hydrocarbons, branched and hyperbranched polymers, and, more generally, molecules with multiple functional groups. In such systems, molecular architecture (e.g., branching) can have an important effect on the thermodynamic properties. For example, it is well known that for hydrocarbons with a given number of carbon atoms branching typically leads to a decrease in the boiling point and critical temperature, and that at a given temperature the cloud point pressure of polymers, such as polyolefins, generally decreases as the degree of polymer branching increases [2]. Similarly the nature of the functional groups in small molecules, and the incorporation of different functional groups and their arrangement into a polymer backbone, can also strongly influence thermodynamic properties and phase behavior. For example, poly(vinyl acetate) (PVAc) is more CO_2-soluble than poly(methyl acrylate) (PMA) due to the position of the carbonyl group in the polymer repeat unit; the PMA and PVAc repeat units both have the same number of carbon, hydrogen, and oxygen atoms, they differ only in the position of the carbonyl group [3].

While experimental thermodynamics and phase behavior data is essential to the development of accurate theoretical tools, experiments alone are unable to quantify the effects of molecular structure and composition on the phase behavior of pure fluids and their mixtures, due to the sheer number of experiments that would be needed for a systematic study. While equations of state (EoS) are today routinely used to calculate thermodynamic properties, cubic equations, which dominate in the study of simple fluids, tend to give poor predictions for complex fluids and their mixtures, such as polymers and associating systems, as they do not explicitly take into account the architecture of the molecules and association interactions. This often results in

* Corresponding author. Tel.: +1 615 322 6853; fax: +1 615 343 7951.
E-mail address: c.mccabe@vanderbilt.edu (C. McCabe).

0378-3812/$ – see front matter © 2008 Elsevier B.V. All rights reserved.
doi:10.1016/j.fluid.2008.11.008

the need for unphysical mixing rules and temperature-dependent and/or concentration-dependent binary interaction parameters. Statistical-mechanics-based EoSs are an attractive alternative since, being molecular-based, the model parameters are related to the molecular shape, size, and interactions of the molecules, and so tend to lead to more robust, predictive approaches.

The statistical associating fluid theory (SAFT) [4,5], based on the seminal work of Wertheim [6–9], is one example of a molecular-based equation of state. Since the introduction of the original SAFT expressions in the late 1980s there are now many versions and applications of SAFT-based approaches reported in the literature; the reader is directed to the excellent reviews of Economou [10] and Müller and Gubbins [11] for an overview. In this work we focus on SAFT-VR in which the dispersion interactions are modelled through a potential of variable attractive range, typically a square-well potential [12,13]. SAFT-VR has been successfully used to describe the fluid phase equilibria of a wide range of industrially important systems; for example, short alkanes through to simple polymers of high-molecular weight [14–20], and their binary mixtures [15,21–28], perfluoroalkanes [29–32] and other fluorinated molecules [33–37], water [38–40], carbon dioxide [26,41–46], and electrolytes [40,47–50] have all been studied.

Within the SAFT-VR approach, and typically with most SAFT-based equations of state, molecules are treated as homo-segmented chains composed of identical tangentially bonded segments. For example, an alkane is generally modeled as a chain of identical segments, the parameters for which are obtained by fitting to vapor pressure and saturated liquid density data. With this approach it is therefore assumed that each alkane has its own individual set of parameters. In order to develop a more predictive approach several authors [16,51–57] have shown that simple empirical relationships for the *n*-alkane parameters can be obtained by correlating the parameters for individual alkanes against molecular weight or the number of carbon atoms. This allows for the extrapolation of the model parameters to long-chain *n*-alkanes, for which limited experimental data are available, and to linear polymers such as polyethylene [17,58]. However, the extension of such techniques beyond polyolefins to functionalized polymers and copolymers has met with limited success (see for example the work of Hasch and McHugh [59]). Additionally, the use of polymer PVT data (in place of the phase coexistence data typically used in fitting model parameters for small molecules) to determine polymer parameters is generally not successful [60–62] and so several alternative methods have been proposed, such as using empirical corrections to the parameters for polyethylene [63] and a combination of fitting to polymer densities and polymer-solvent cloud point data [64,65]. Pseudo-group-contribution type approaches, which we denote as "group-averaging" approaches, have also been proposed in which the values for m and σ are typically obtained from a linear summation of the values for characteristic groups defined in the molecule and the energy parameters determined from either a fit to vapor pressure and liquid density data for the monomer, and then used for the corresponding polymer, or from a fit to binary cloud point data [66]. A common feature of these, and similar, studies is the necessarily *ad hoc* way in which parameters are put together, which no doubt impacts the need to use pure component and/or cross parameters fitted to experimental mixture data, and so limits predictive capability. The rational for group-averaging is the perception that thermodynamic properties are not as sensitive to the details of the group–group interactions and their placement within the molecule.

In an effort to develop a more predictive model, and reduce the reliance on experimental data, we have combined the hetero-SAFT-VR approach [67,68] that allows the study of chains composed of segments of different size and/or energy parameters, with a group-contribution approach that defines key functional groups to develop the group-contribution SAFT-VR (GC-SAFT-VR) equation. The GC-SAFT-VR approach allows us to accurately capture the nature of the molecular structure, including branching, and type and location of functional groups within a molecule, through the use of a heteronuclear chain model in which the definition of different segments in the molecular model is retained and their connectivity specified. Once parameters have been determined for a wide range of functional groups, within the GC-SAFT-VR approach we can easily determine the model parameters for new molecules and polymers containing those functional groups, providing a consistent means by which to determine model parameters and a predictive approach to studying their thermodynamics and phase behavior.

In similar work, Tobaly et al. [69–73] have proposed a group-contribution SAFT-based equation of state (GC-SAFT), in which representative groups are defined according to a molecules composition and structure; however the parameters for each group are then averaged over the whole molecule (i.e., group-averaged), which is then represented as a homo-segmented monomer fluid and model chain. The GC-SAFT method has been tested using the original SAFT [5], PC-SAFT [74], and SAFT-VR [12] equations and applied to study the phase behavior of pure linear hydrocarbons [69], linear alcohols [69] and their binary mixtures [70], esters [71] and binary mixtures of H_2 + *n*-alkanes, CO_2 + *n*-alkanes [72] and polymer systems [73]. More recently, Lymperiadis et al. [75] have developed a group-contribution approach based on the SAFT-VR equation, which describes a hetero-segmented monomer fluid from which effective parameters are then obtained and molecules formed from homo-segmented fused, rather than tangent, chains.

In this work, we propose a group-contribution method based on the hetero-SAFT-VR EoS [67,68] in order to develop a more physically realistic model for real fluids, i.e., one in which the segments of the model chain can have different size and/or energy parameters in order to mimic the natural heterogeneity of real molecules. We find that our approach allows a quantitative description of the effects of molecular architecture and molecular composition on the thermodynamic properties of fluids, and provides a clear way to determine parameters for polymers based on the functional groups in the repeat unit. The remainder of the paper is organized as follows. In Section 2 we provide a description of the molecular model used and outline the GC-SAFT-VR equation; details of the parameter regression and results for alkanes, branched alkanes, 1-alkenes, ketones, alkylbenzene, esters and their binary mixtures are presented in Section 3; finally conclusions are drawn and future work discussed in Section 4.

2. Model and theory

The GC-SAFT-VR approach models fluids as chains composed of tangentially bonded segments that represent different functional groups. As in the SAFT-VR approach, the segments representing each different type of functional group, interact via a square-well potential that is characterized by three parameters; the segment diameter σ, well depth ε, and potential range λ. The free energy of the fluid is written as the sum of four separate contributions:

$$a = a^{ideal} + a^{mono} + a^{chain} + a^{assoc} \quad (1)$$

where a^{ideal} is the ideal free energy, a^{mono} the contribution to the free energy due to the monomer segments, a^{chain} the contribution due to the formation of bonds between monomer segments, and a^{assoc} the contribution due to association interactions. The expressions for a^{assoc} are not included in this work since the systems studied here are not associating fluids. The expressions for each of the remaining terms for a mixture system composed of hetero-segmented chain molecules are presented below. We note that the

equations for pure hetero-segmented fluids in the hetero-SAFT-VR approach were presented in a previous publication by the authors [68].

The ideal Helmholtz free energy is given by

$$\frac{A^{ideal}}{NkT} = \sum_{k=1}^{n} x_k \ln \rho_k \Lambda_k^3 - 1 \tag{2}$$

where n represents the number of pure components, $\rho_k = (N_k/V)$ the molecular number density of component k, where N_k is the number of molecules of component k and V the volume, x_k the mole fractions of component k in the mixture, and Λ_k the thermal de Broglie wavelength.

The monomer free energy is given by a second-order high-temperature expansion using Barker and Henderson perturbation theory for mixtures [76], viz

$$\frac{A^{mono}}{NkT} = \sum_{k=1}^{n}\sum_{i=1}^{n'_k} x_k m_{ki}(a^{HS} + \beta a_1 + \beta^2 a_2) \tag{3}$$

where n'_k is the number of types of functional groups in a component k and $m_{ki} = \nu_{ki} m_i$, where ν_{ki} is the number of functional groups of type i present in component k and m_i the chain length of functional group type i.

The hard sphere reference term a^{HS} is determined from the expression of Boublik [77] and Mansoori and co-workers [78] for multicomponent hard sphere systems, viz

$$a^{HS} = \frac{6}{\pi\rho_s}\left[\left(\frac{\zeta_2^3}{\zeta_3^2} - \zeta_0\right)\ln(1-\zeta_3) + \frac{3\zeta_1\zeta_2}{1-\zeta_3} + \frac{\zeta_2^3}{\zeta_3(1-\zeta_3)^2}\right] \tag{4}$$

where ρ_s is the total number density of segments, defined as N_s/V, where N_s is the total number of segments, and ζ_l is the reduced density given by a sum over all segments:

$$\zeta_l = \frac{\pi}{6}\rho_s\left[\sum_{k=1}^{n}\sum_{i=1}^{n'_k} x_{s,ki}(\sigma_{ki,ki})^l\right], \quad l = 0, 1, 2, 3 \tag{5}$$

where $\sigma_{ki,ki}$ is the diameter of segments of type i in chain k and $x_{s,ki}$ the mole fraction of segments of type i in chain k, expressed as

$$x_{s,ki} = \frac{x_k m_{ki}}{\sum_{k=1}^{n}\sum_{i=1}^{n'_k} x_k m_{ki}} \tag{6}$$

The first perturbation term (a_1) describing the mean-attractive energy is obtained from the sum of all pair interactions:

$$a_1 = \sum_{l=1}^{n}\sum_{j=1}^{n'_l}\sum_{k=1}^{n}\sum_{i=1}^{n'_k} x_{s,ki}x_{s,lj}(a_1)_{ki,lj} \tag{7}$$

where $(a_1)_{ki,lj}$ is obtained from the mean-value theorem as proposed by Gil-Villegas et al. [12] and expressed through the hard sphere radial distribution function $g_0^{HS}[\sigma_x; \zeta_x^{eff}(\lambda_{ki,lj})]$ using the van der Waals one fluid theory:

$$\begin{aligned}(a_1)_{ki,lj} &= -2\pi\rho_s\varepsilon_{ki,lj}\int_{\sigma_{ki,lj}}^{\infty} r_{ki,lj}^2 g_{ki,lj}^{HS}(r_{ki,lj})\,dr_{ki,lj} \\ &= -\rho_s\frac{2\pi}{3}\sigma_{ki,lj}^3\varepsilon_{ki,lj}(\lambda_{ki,lj}^3 - 1)g_{ki,lj}^{HS}(\sigma_{ki,lj}; \zeta_3^{eff}) \\ &= -\rho_s\frac{2\pi}{3}\sigma_{ki,lj}^3\varepsilon_{ki,lj}(\lambda_{ki,lj}^3 - 1)g_0^{HS}[\sigma_x; \zeta_x^{eff}(\lambda_{ki,lj})]\end{aligned} \tag{8}$$

where $g_0^{HS}(\sigma_x; \zeta_x^{eff})$ is obtained from the Carnahan and Starling equation of state [79]:

$$g_0^{HS}[\sigma_x; \zeta_x^{eff}(\lambda_{ki,lj})] = \frac{1 - \zeta_x^{eff}/2}{(1-\zeta_x^{eff})^3} \tag{9}$$

and the expression for the effective packing fraction ζ_x^{eff} is obtained from the Padé expression proposed by Patel et al. [80]:

$$\zeta_x^{eff} = \frac{C_1\zeta_x + C_2\zeta_x^2}{(1 + C_3\zeta_x)^3} \tag{10}$$

$$\begin{pmatrix} c_1 \\ c_2 \\ c_3 \end{pmatrix} = \begin{pmatrix} -3.16492 & 13.35007 & -14.80567 & 5.70286 \\ 43.00422 & -191.66232 & 273.89683 & -128.93337 \\ 65.04194 & -266.46273 & 361.04309 & -162.69963 \end{pmatrix} \times \begin{pmatrix} \dfrac{1}{\lambda_{ki,lj}} \\ \dfrac{1}{\lambda_{ki,lj}^2} \\ \dfrac{1}{\lambda_{ki,lj}^3} \\ \dfrac{1}{\lambda_{ki,lj}^4} \end{pmatrix} \tag{11}$$

where

$$\zeta_x = \frac{\pi}{6}\rho_s\sigma_x^3 = \frac{\pi}{6}\rho_s\sum_{l=1}^{n}\sum_{j=1}^{n'_l}\sum_{k=1}^{n}\sum_{i=1}^{n'_k} x_{s,ki}x_{s,lj}\sigma_{ki,lj}^3 \tag{12}$$

The second-order perturbation term for the monomer excess free energy a_2 is expressed as

$$a_2 = \sum_{l=1}^{n}\sum_{j=1}^{n'_l}\sum_{k=1}^{n}\sum_{i=1}^{n'_k} x_{s,ki}x_{s,lj}(a_2)_{ki,lj} \tag{13}$$

where $(a_2)_{ki,lj}$ is obtained through the local compressibility approximation:

$$(a_2)_{ki,lj} = \frac{1}{2}K^{HS}\varepsilon_{ki,lj}\rho_s\frac{\partial(a_1)_{ki,lj}}{\partial\rho_s} \tag{14}$$

and K^{HS} is the Percus-Yevick expression for the hard-sphere isothermal compressibility:

$$K^{HS} = \frac{\zeta_0(1-\zeta_3)^4}{\zeta_0(1-\zeta_3)^2 + 6\zeta_1\zeta_2(1-\zeta_3) + 9\zeta_2^3} \tag{15}$$

Finally the contribution to the free energy due to chain formation from a mixture of hetero-segmented square-well monomer segments is given by

$$\frac{A^{chain}}{NkT} = -\sum_{k=1}^{n} x_k \sum_{ij} \ln y_{ki,kj}^{SW}(\sigma_{ki,kj}) \tag{16}$$

where the first sum is over all components in the mixture and the second sum considers the chain formation and connectivity of the segments within a given chain. The background correlation function is given by

$$y_{ki,kj}^{SW}(\sigma_{ki,kj}) = \exp(-\beta\varepsilon_{ki,kj})g_{ki,kj}^{SW}(\sigma_{ki,kj}) \tag{17}$$

where $g_{ki,kj}^{SW}(\sigma_{ki,kj})$ is the radial distribution function for the square-well monomers and is approximated by a first-order high-temperature perturbation expansion [12]. The exact form of Eq. (16) depends on the number of different types of segments and connectivity in the molecules being studied. For example, if we consider a

Table 1
GC-SAFT-VR parameters for the segment size and segment number of each group studied.

Groups	σ (Å)	m_i
CH_3	3.737	0.667
CH_2	4.041	0.333
CH	3.925	0.100
C=O	3.496	0.580
CH_2=CH	3.574	1.052
C_6H_5	3.158	2.693
OCH_2	2.950	1.000
OCH_3	3.078	1.330

Table 3
GC-SAFT-VR segment–segment energy range parameters λ_{ij}.

Type	CH_3	CH_2	CH	C=O	CH_2=CH	C_6H_5	OCH_2	OCH_3
CH_3	1.492	1.583	1.725	1.685	1.529	1.734	1.546	1.566
CH_2	1.583	1.667	1.804	1.586	1.621	1.822	1.645	1.662
CH	1.725	1.804	1.946	1.920*	1.766*	1.979*	1.804*	1.818*
C=O	1.685	1.586	1.920*	1.891	1.728*	1.953*	1.764	1.558
CH_2=CH	1.529	1.621	1.766*	1.728*	1.568	1.781*	1.589*	1.608*
C_6H_5	1.734	1.822	1.979*	1.953*	1.781*	2.021	1.824*	1.840*
OCH_2	1.546	1.645	1.804*	1.764	1.589*	1.824*	1.614	1.635*
OCH_3	1.566	1.662	1.818*	1.558	1.608*	1.840*	1.635*	1.655

* Assumes Lorentz-Berthelot combining rules. Cross interaction not yet tested.

binary mixture of *n*-alkanes such as the *n*-hexane + *n*-hexadecane system studied in this work. *n*-Alkanes are composed of two types of functional groups, CH_3 which we denote as segments of type 1 with molecular parameters m_1, $\sigma_{k1,k1}$, $\varepsilon_{k1,k1}$, $\lambda_{k1,k1}$ and CH_2 which we denote as segments of type 2 with molecular parameters m_2, $\sigma_{k2,k2}$, $\varepsilon_{k2,k2}$, $\lambda_{k2,k2}$. The *n*-hexane molecule has 2 CH_3 functional groups, 4 CH_2 groups, 2 bonds between these functional groups (CH_2–CH_3) and 3 bonds between CH_2–CH_2 groups; in the case of the *n*-hexadecane molecule, similar to *n*-hexane, it has 2 CH_3 functional groups, 2 connections between the CH_2 and CH_3 groups, 14, rather than 4 CH_2 groups, and 13 bonds between CH_2–CH_2 groups. In this case, Eq. (16) is given by

$$\frac{A^{chain}}{NkT} = -x_1[2\ln y^{SW}_{11,12}(\sigma_{11,12}) + (2m_1 - 2)\ln y^{SW}_{11,11}(\sigma_{11,11}) + (4m_2 - 1)\ln y^{SW}_{12,12}(\sigma_{12,12})] - x_2[2\ln y^{SW}_{21,22}(\sigma_{21,22}) + (2m_1 - 2)\ln y^{SW}_{21,21}(\sigma_{21,21}) + (14m_2 - 1)\ln y^{SW}_{22,22}(\sigma_{22,22})] \quad (18)$$

where the first term in square brackets describes the *n*-hexane and within this contribution the terms correspond to; the two bonds between segments of type 1 and type 2 ($2\ln y^{SW}_{11,12}(\sigma_{11,12})$), the three bonds between segments of type 2 ($3\ln y^{SW}_{12,12}(\sigma_{12,12})$), the chain formation contribution from the two CH_3 groups ($(2m_1 - 2)\ln y^{SW}_{11,11}(\sigma_{11,11})$) and the chain formation contribution from the four CH_2 groups ($(4m_2 - 4)\ln y^{SW}_{12,12}(\sigma_{12,12})$). The second term in square brackets corresponds to the *n*-hexadecane. Note that since *n*-hexane and *n*-hexadecane have similar functional groups, the values of $\sigma_{11,11} = \sigma_{21,21}$, $\sigma_{12,12} = \sigma_{22,22}$ and $\sigma_{11,12} = \sigma_{21,22}$.

3. Results

We have developed the GC-SAFT-VR approach and in this initial study determined the molecular parameters for eight classes of functional groups by fitting to experimental data for selected members of different chemical families, namely *n*-alkanes, branched alkanes, 1-alkenes, ketones, alkylbenzenes, alkyl acetates and methyl esters using an annealing technique [81,82]. We first examine the phase behavior for each class of pure fluids using the GC-SAFT-VR approach and illustrate the transferability of the group parameters determined through the study of the phase behavior of molecules not included in the fitting process. The parameters determined for each functional group are reported in Tables 1–3 and the percentages of absolute average deviation of the vapor pressure (*%AAD P*) and liquid density (*%AAD* ρ_{Liq}) from the experimental values obtained for both the correlated and predicted phase behavior are presented in Appendix A (Tables A.1–A.7). In all cases the range of experimental data considered excluded points near the critical region (since the GC-SAFT-VR approach will over predict the critical point as discussed below) and vapor pressures near the triple point. The choice of molecules used in the fitting process for each system is dictated by the availability of experimental data; for each class of family studied we have chosen a representative sample of molecules to be included in the fitting process, whilst still reserving some data to compare predictions from the model to. Once the new approach has been tested and validated for pure fluids we then predict, without any additional fitting to experimental data, the phase behavior of a number of binary mixtures, which further demonstrates the versatility and accuracy of the GC-SAFT-VR approach and the importance of using a more physically based model.

3.1. Pure fluids

As discussed above, in the GC-SAFT-VR approach we describe *n*-alkanes as chains composed of two types of segments or functional groups (CH_2 and CH_3), the parameters for which are obtained by fitting to experimental data for selected alkanes, namely propane (C_3H_8) to *n*-decane ($C_{10}H_{22}$), *n*-dodecane ($C_{12}H_{26}$), *n*-hexadecane ($C_{16}H_{34}$), and *n*-eicosane ($C_{20}H_{42}$). Methane and ethane were naturally excluded from the fitting process due to their size and anomalous properties and heavier compounds were included in order to obtain parameters suitable for both light and heavy alkanes. In order to reduce the number of fitted parameters for the hydrocarbon groups we determined the number of segments *m* in the model chain from the simple relationship:

$$m = \frac{1}{3}(C - 1) + 1 \quad (19)$$

which has proven to provide a good description of the critical temperatures and pressures of linear alkanes [83,84] and has been

Table 2
GC-SAFT-VR segment–segment energy well depth parameters ε_{ij}/k_B (K).

Type	CH_3	CH_2	CH	C=O	CH_2=CH	C_6H_5	OCH_2	OCH_3
CH_3	234.250	235.735	153.064	307.223	226.675	165.521	157.702	191.144
CH_2	235.735	237.230	154.034	309.171	228.112	166.570	158.702	192.356
CH	153.064	154.034	100.015	200.746*	148.114*	108.155*	103.046*	124.897*
C=O	307.223	309.171	200.746*	402.929	297.288*	217.084*	206.829	250.689
CH_2=CH	226.675	228.112	148.114*	297.288*	219.344	160.168*	152.602*	184.962*
C_6H_5	165.521	166.570	108.155*	217.084*	160.168*	116.957	111.432*	135.062*
OCH_2	157.702	158.702	103.046*	206.829	152.602*	111.432*	106.168	128.682*
OCH_3	191.144	192.356	124.897*	250.689	184.962*	135.062*	128.682*	155.970

* Assumes Lorentz-Berthelot combining rules. Cross interaction not yet tested.

widely adopted in SAFT studies of *n*-alkanes. In the long chain limit Eq. (19) gives a value of m for a methylene group (CH_2) of 0.333, and since the total number of segments in the *n*-alkane molecule is equal to

$$m = 2m_{CH_3} + (C-2)m_{CH_2} \quad (20)$$

where C is the number of carbon atoms, the value of m for the methyl group (CH_3) can easily be calculated as $m_{CH_3} = 0.667$. The remaining parameters for the CH_2 and CH_3 groups, and their cross interactions, are given in Tables 1–3 for the segment size, potential well depth and width, respectively. We note that for the alkanes and other hydrocarbon systems studied the cross interactions are given by the Lorentz-Berthelot mixing rules, however for cross interactions between non-polar and polar groups, we might expect deviations from Lorentz-Berthelot combining rules to be observed. In cases where the Lorentz-Berthelot combining rules fail, in contrast to traditional equation of state and SAFT-based approaches, we can fit the cross interactions to pure component experimental data. In this work, only the cross interaction parameters between CH_2/C=O and OCH_3/C=O groups present in ketones and esters were fitted to pure component experimental data. We also note that the parameters determined for the CH_2 group are very close to those determined from simple empirical relations for the SAFT-VR parameters as a function of molecular weight [20]. The *%AAD* obtained with the GC-SAFT-VR approach for the vapor pressure and saturated liquid density are reported in Table A.1; for the *n*-alkanes used in the fitting process we find that the overall average deviation for vapor pressure is 5.76% and for the liquid densities is 2.95%. The results for propane, the smallest *n*-alkane molecule considered, showed the highest *%AAD* value due to the dominant influence of the CH_3 groups. Although the agreement with experimental data is not as accurate as that obtained by fitting parameters separately for each alkane, we do find that our results are generally more accurate than those obtained when using parameters determined from correlations of the SAFT-VR parameters with molecular weight or carbon number [20]; for comparison the *%AAD* values for results obtained from the empirical expressions of Paricaud et al. [20] are also reported in Table A.1 and overall show larger deviations in the vapor pressures (11.11%) but are comparable in the liquid densities (2.40%). Although not reported in Table A.1, we note that similar behavior is observed if the expressions proposed by McCabe et al. are used [16]. A direct comparison of our results with previous work on group-contribution approaches [69–73,75] is more difficult since many factors contribute to the calculations of the *%AAD*'s, such as which substances are correlated versus predicted, which substances are included in the fitting process and the range of the experimental thermodynamic data used, as well as which version of SAFT is used as the underlying model and the flexibility of the resulting group-contribution approach; therefore, only a qualitative comparison is possible. For example, for the *n*-alkanes Tamouza et al. [69] obtained an overall deviation for the vapor pressure and saturated liquid density of 1.68% and 2.24%, respectively, which is lower than the values reported in Table A.1; however in the fitting process only experimental data for *n*-alkanes up to *n*-decane were included while in the current work longer alkanes such as *n*-dodecane, *n*-hexadecane and *n*-eicosane were also considered. Additionally in the experimental data used in the fitting process we considered a wider temperature range, including more data at low temperatures which also contributes to the observed deviations as discussed in the work of Lafitte et al. [85] who showed that better agreement can be obtained if experimental data near the triple point is not included in the parameter estimation. Similarly, only a qualitative comparison can be made with the work of Lymperiadis et al. [75] who obtained deviations of 3.98% for the vapor pressure and 0.57% for the saturated liquid density by again only fitting data for the *n*-alkanes up to *n*-decane.

Having presented the agreement with experimental data for correlated *n*-alkanes we now test the transferability of the functional group parameters obtained for the GC-SAFT-VR approach by studying the phase diagrams of heavier alkanes, not included in the fitting process. Predictions for the vapor pressures and saturated liquid densities of *n*-undecane ($C_{11}H_{24}$) to *n*-hexatriacontane ($C_{36}H_{74}$) are compared with experimental data and the corresponding *%AAD* values for the vapor pressures and liquid densities are reported in Table A.1. Generally, we find that the deviations between the GC-SAFT-VR predictions and experimental data for the saturated liquid density are much smaller than those obtained for predictions for the vapor pressure, indicating that the vapor pressure is a more sensitive quantity. For comparison we again provide *%AAD* P^* and *%AAD* ρ^*_{Liq} values for the SAFT-VR description of these *n*-alkanes obtained using correlations from the work of Paricaud et al. [20]. Here both models provide similar deviations in the description of the phase behavior of these systems. We note that in comparison to the work of Tamouza et al. [69] and Lymperiadis et al. [75] the GC-SAFT-VR approach has been applied to the prediction of a much wider range of hydrocarbon molecules and in general the agreement with experimental data is again comparable between the different approaches; Tamouza et al. achieve lower deviations with experimental data for the vapor pressure of the selected *n*-alkanes studied compared to the GC-SAFT-VR approach and Lymperiadis et al. achieve lower density deviations compared to GC-SAFT-VR.

In order to describe branched alkanes a CH group needs to be defined. The parameters for the CH group were determined by fitting to vapor pressure and saturated liquid density data for two families of branched alkanes, methylalkanes and ethylalkanes, while using the CH_2 and CH_3 group parameters already determined. The deviations between the GC-SAFT-VR description of the phase diagrams and experimental data are reported in Table A.2 and the parameters obtained for the CH group given in Tables 1–3. In contrast to the linear alkane family, we fitted all the molecular parameters for the CH group whilst also ensuring that the parameters for the CH_3, CH_2 and CH groups make physical sense. In Fig. 1 we present the molecular parameters obtained for the CH group together with those of the other *n*-alkane groups as a function of molecular weight, which illustrates that the parameters for the CH group fall within the trend of the parameters for the CH_3 and CH_2 groups. From Table A.2 we note that the agreement with experimental data is good, with an overall deviation from experimental data for the liquid densities of 3.96% and 6.46% for the vapor pressures. As a test of the theory, we have also studied several branched alkanes not included in the fitting process. Results for 2-methyl heptane, three dimethyl-branched alkanes, and squalane are presented in Table A.2. The theory is able to describe the phase behavior as we change the branched compound, although an over-prediction of the experimental data is seen for squalane, which is a highly branched isomer of C_{30} (2,6,10,15,19,23-hexamethyltetracosane) and could be due to the flexible nature of the SAFT model. We find that the liquid density of these systems is very well predicted by the GC-SAFT-VR approach, although the agreement with experimental data is poor close to the critical point as expected for a classical EoS that does not consider the long-range density fluctuations that occur in this region. This can be addressed through the incorporation of so-called crossover techniques into the SAFT-VR equation of state [19,25,26], however this is beyond the scope of the present work. We note however that the agreement in the liquid density for squalane is very good given that the parameters used to predict the phase diagram are fitted to linear *n*-alkanes and a small number of singly branched alkanes.

In order to study unsaturated alkanes such as 1-alkenes another functional group needs to be defined to incorporate the unsaturated carbon bond. The parameters for the CH_2=CH group were determined by fitting to experimental vapor pressure and saturated

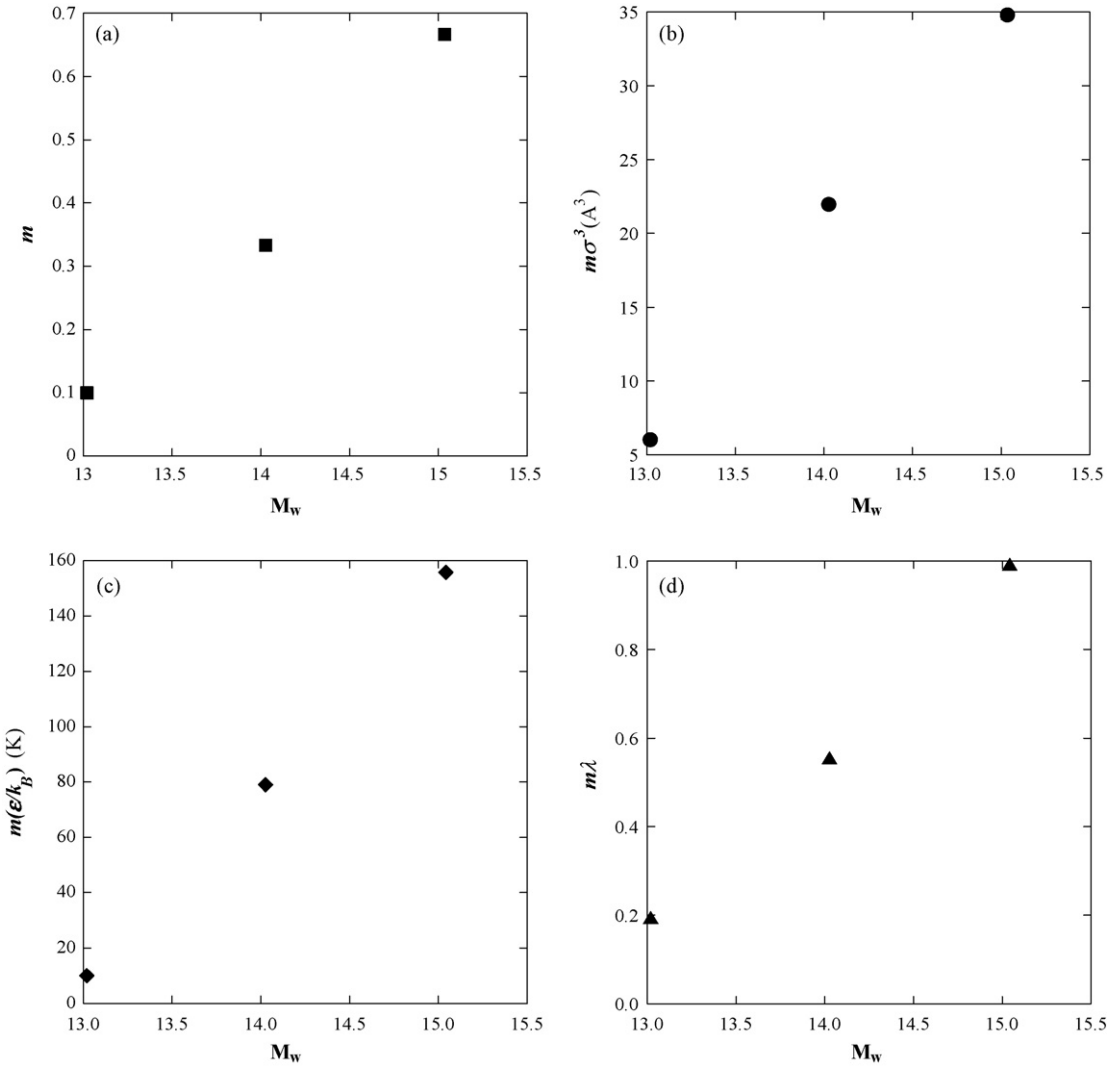

Fig. 1. GC-SAFT-VR molecular parameters for the functional groups CH_3, CH_2 and CH as a function of the molecular weight: (a) chain length, (b) segment size, (c) potential depth and (d) potential range.

liquid density data for eight 1-alkenes from propene to 1-decene while using the CH_2 and CH_3 groups previously defined to describe the other functional groups present in the 1-alkene molecules. As can be seen from the *%AAD* values given in Table A.3, good agreement with the experimental data is obtained, with an overall *%AAD* of 4.02% for the vapor pressure and 2.60% for the saturated liquid density. In order to test the transferability of the parameters for the CH_2=CH group, we have also studied the phase behavior of longer 1-alkenes, from 1-undecene up to 1-eicosene. For these systems, we report *%AAD* values for the predictions of the vapor pressure and liquid densities in Table A.3 that are in good agreement with the experimental data, obtaining similar *%AAD* values to those reported for the shorter 1-alkenes.

Having defined parameters for the groups forming the "backbone" of organic molecules we can now define parameters for common functional groups in other classes of organic molecules. In this initial study we have focused on alkylbenzenes, ketones, and esters since the benzenyl (C_6H_5), carbonyl (C=O), and ester groups (OCH_2 and OCH_3) are common functional groups in polymers. In order to determine parameters for the benzenyl group (C_6H_5) we studied alkylbenzenes, which can be represented by a benzenyl group bonded to a linear alkyl chain formed from CH_2 and CH_3 groups. Short alkylbenzene molecules from methylbenzene to decylbenzene were selected for regression of the model parameters for the benzenyl group (C_6H_5). The *%AAD* values obtained for the systems studied in the fitting process are reported in Table A.4. For this functional group the overall deviation of the theoretical results from the experimental data is 4.70% and 3.76% for the vapor pressure and saturated liquid density, respectively. Within this chemical family, we note that the shape of the predicted liquid density is less curved than that observed experimentally, which could be due to the description of the C_6H_5 group as a single entity. Extensive *ab initio* calculations have shown that the strength of the π–π interactions between two aromatic rings can be explained (and modeled) by the large number of atom–atom interactions between the atoms in the two rings, and that this is also the source of its the directionality (i.e., the favoring of the parallel stacked configuration over other relative orientations) [86]. This might suggest that a more accurate group-contribution model for the benzene group would involve decomposition of the ring into CH groups; however, we note that similar deviations from experimental data are seen in the SAFT-γ approach which models the benzene ring by several fused segments [75]. An alternative explanation could be that the quadrupolar interactions are not explicitly included in the model, which has been addressed in the work of NguyenHuynh et al. [87].

In order to test the transferability of the benzenyl group parameters, we use the same set of parameters to now examine the phase behavior of longer alkylbenzene systems, from undecylbenzene

up to octadecylbenzene. From Table A.4 we see that the deviations between the predicted vapor pressures and experimental data become larger as the alkyl chain increases, though good agreement is achieved in all cases for the saturated liquid density.

Having examined the CH_3, CH_2, CH, CH_2=CH, and C_6H_5 groups, which allow us to study alkanes, alkenes, and alkylbenzenes we now consider ketones and esters. In order to determine parameters for the carbonyl group we fitted to experimental vapor pressure and saturated liquid density data for selected symmetric ketones (3-pentanone, 3-hexanone, 4-heptanone, 4-octanone, 5-nonanone) in which the carbonyl group lies in the center of the ketone chain. Ketones have strong dipolar interactions due to the carbonyl group and so we would expect the cross carbonyl–alkyl interaction to deviate from the Lorentz-Berthelot combining rules; during the regression process it was found that tuning just the cross range parameter away from its Lorentz-Berthelot value enabled good agreement with experimental data to be obtained. The regressed intermolecular parameters for the functional group C=O are presented in Tables 1–3 and the *%AAD* values obtained in the fitting procedure are reported in Table A.5, giving an overall deviation of 5.76% and 1.57% for vapor pressure and saturated liquid density, respectively. The transferability of the carbonyl group parameters was then tested through the prediction of the phase diagrams of 6-undecanone, 8-pentadecanone, and 16-hentriacontanone as reported in Table A.5. As can be seen, the theoretical predictions are in good agreement with the experimental data, giving an overall *%AAD* of 4.15% for the vapor pressures and 1.32% for the saturated liquid densities.

In order to model esters two new groups, OCH_2 and OCH_3, need to be defined to describe the oxygen atom that is located next to the carbonyl group. For the OCH_2 functional group the vapor pressure and saturated liquid density of alkyl acetates from propyl acetate up to nonyl acetate were used in the parameter regression, which is performed while keeping the parameters for the CH_2, CH_3, and C=O groups and their cross interactions fixed to the previously determined values. The regressed parameters are presented in Tables 1–3 and the corresponding *%AAD* values are reported in Table A.6. For the ester molecules studied both the vapor pressure and saturated liquid densities are correlated very well in comparison to the experimental data, showing overall *%AADs* of 6.90% and 2.22% for vapor pressure and saturated liquid density, respectively. The transferability of the fitted parameters for the OCH_2 group were again then tested by comparing the GC-SAFT-VR predictions with experimental data for pure ester systems not included in the fitting process. Specifically we studied the phase equilibria of ethyl butanoate, butyl pentanoate and butyl nonanoate that have longer alkyl chains and diethyl succinate, which has two carbonyl and ester groups (C=O and OCH_2). As shown in Table A.6, the results provide a good quantitative prediction of the experimental saturated liquid density data (an overall *%AAD* of 1.60%), but only qualitative agreement is achieved with the experimental vapor pressures as we increase the length of the acetate alkyl chain. Since an improved agreement could not be obtained by tuning the cross interaction parameters, it may be necessary to include an explicit treatment of the dipolar interactions into the GC-SAFT-VR approach using the recently developed SAFT-VR+D equation [88] for such polar fluids.

The last functional group studied is the OCH_3 group found in methyl esters. In the GC-SAFT-VR approach the methyl esters are modeled as a chain composed of one OCH_3 group connected to a carbonyl group (C=O) that is in turn connected to an alkyl chain formed from CH_2 and CH_3 functional groups. The set of intermolecular parameters for the OCH_3 group have been fitted to experimental data for the vapor pressure and saturated liquid density of a selected group of short methyl esters, ranging from methyl ethanoate up to methyl decanoate. The *%AAD* values obtained in the fitting process are reported in Table A.7 from which we can see that the

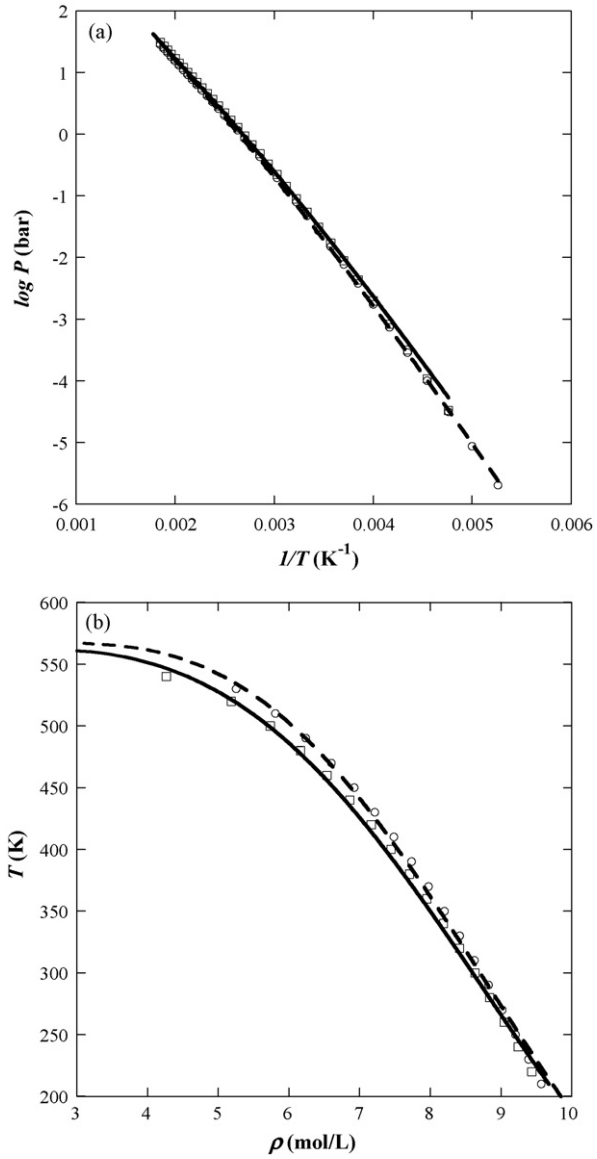

Fig. 2. Comparison between theoretical results using the GC-SAFT-VR approach and experimental data [90] for (a) the vapor pressure and (b) the saturated liquid density of two ester isomers: methyl butanoate (dashed lines and circles) and ethyl propanoate (solid lines and squares). The results for methyl butanoate are from a correlation of the experimental data to determine the ester group parameters while those for ethyl propanoate are a prediction from the GC-SAFT-VR equation.

agreement with experimental data is again good, with an overall deviation of 1.28% for the liquid density and 5.49% for the vapor pressure. The higher deviation observed for the vapor pressure can be attributed to the inclusion of two short chain methyl esters, i.e., methyl ethanoate and methyl propanoate for which the highest deviations were obtained and is no doubt due to the terminal groups having a dominant influence.

An advantage of the GC-SAFT-VR approach is that by defining different functional groups and specifying their connectivity we are able to distinguish between some structural isomers. In Fig. 2, we compare the phase behavior for two ester isomers, ethyl propanoate (CH_3CH_2C=OOCH_2CH_3) and methyl butanoate ($CH_3CH_2CH_2C$=OOCH_3), which are modeled using the ester OCH_2 and OCH_3 groups, respectively. From the figure we note that both substances show good agreement with experimental data and that the theory is able to capture the small differences in density between the two isomers; which is particularly impressive when

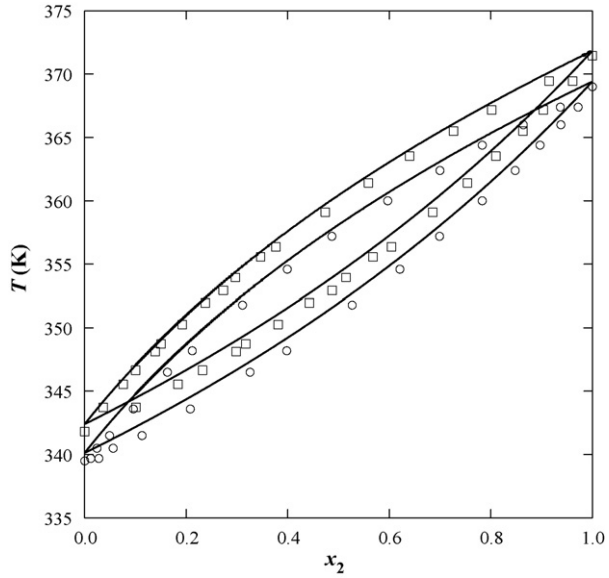

Fig. 3. Predicted constant-pressure *Tx* slices of the *n*-hexane (1) + *n*-heptane (2) phase diagram from the GC-SAFT-VR equation compared with experimental data at 0.94 bar [93,94] (circles) and 1.01 bar (squares).

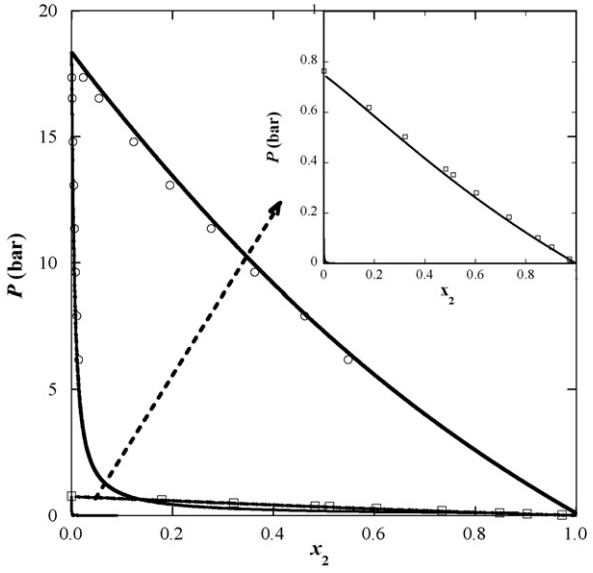

Fig. 4. Predicted constant-temperature *Px* slices of the *n*-hexane (1) + *n*-hexadecane (2) phase diagram from the GC-SAFT-VR equation compared with experimental data [95,96] at 333.15 K (squares) and 472.3 K (circles).

we consider the fact that ethyl propanoate was not included in the fitting process. Additionally, the theory is also able to predict the experimentally observed trend in the boiling points of these esters; the boiling temperature of ethyl propanoate, predicted at 372.92 K compared to 372 K experimentally, is lower than that of methyl butanoate at 378.05 K compared to 376 experimentally [89]. We note however that when describing other structural isomers that contain the same functional groups and number of contacts between the different functional groups, such as *n*-butyl propanoate ($CH_3CH_2C{=}OOCH_2CH_2CH_2CH_3$) and propyl butanoate ($CH_3CH_2CH_2C{=}OOCH_2CH_2CH_3$), the model would not make a distinction between these isomers and the thermodynamic behavior would be the same for both molecules.

3.2. Binary mixtures

Having studied the phase behavior of pure fluids using the GC-SAFT-VR equation and tested the predictive capability of the approach and functional groups defined by studying the phase behavior of other molecules within the same chemical family, but not included in the fitting process, we now turn to the phase behavior of binary mixtures. We present results for selected binary mixtures from the classes of pure components studied including mixtures of *n*-alkanes, alkylbenzenes, *n*-alkanes + alkylbenzenes, *n*-alkanes + ketones, *n*-alkanes + esters, and mixtures of esters.

We first investigate the phase behavior of binary mixtures of *n*-alkanes. For these systems, only two types of groups (CH_3 and CH_2) are used to represent each component, the parameters for which were taken from the pure *n*-alkanes determined as described above, without fitting to any mixture experimental data. Here we illustrate the accuracy of the approach for binary mixtures and present results for just two systems of linear alkanes, since alkane phase behavior can be regarded as somewhat straight forward. The systems chosen are *n*-hexane + *n*-heptane, which is an almost symmetric system in terms of chain length, and *n*-hexane + *n*-hexadecane, which is very asymmetric. In Fig. 3 we present results for constant pressure *Tx* slices of the *n*-hexane + *n*-heptane phase diagram, from which we note an excellent agreement between the theoretical predictions and experimental data. Similar agreement is obtained for the *n*-hexane + *n*-hexadecane system as shown in Fig. 4, where we present constant temperature *Px* slices of the phase diagram over a wide temperature range. While fixing the chain length of component one (hexane) and simply increasing the number of CH_2 groups in the molecular model for component two we see that the theory accurately captures the changes in the phase diagram due to the molecular asymmetry.

We now consider binary mixtures involving alkylbenzenes. In particular, the binary mixture of ethylbenzene + *n*-alkanes and ethylbenzene + propylbenzene and butylbenzene were studied. In Fig. 5, the phase behavior of ethylbenzene with *n*-heptane and *n*-octane at 1 bar is shown. It can be seen from the figure that the theory is able to correctly predict the different phase behavior seen in the ethylbenzene + *n*-alkane mixtures as we vary the linear alkane from heptane to octane; however, the theoretical predictions exhibit a slight deviation from experimental data as we increase the molar composition of ethylbenzene, due to the fact that the vapor pressure of pure ethylbenzene (see Table A.4) is

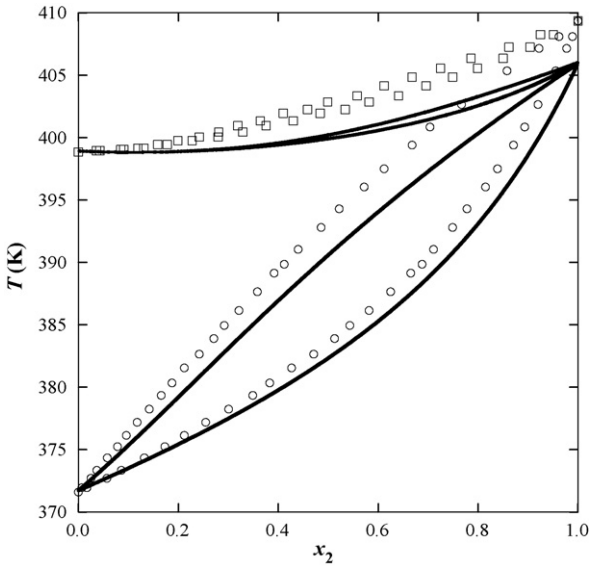

Fig. 5. Predicted constant-pressure *Tx* slices of the *n*-heptane (1) + ethylbenzene (2) (circles) and *n*-octane (1) + ethylbenzene (2) (squares) phase diagrams from the GC-SAFT-VR equation compared with experimental data [97,98] at 1 bar.

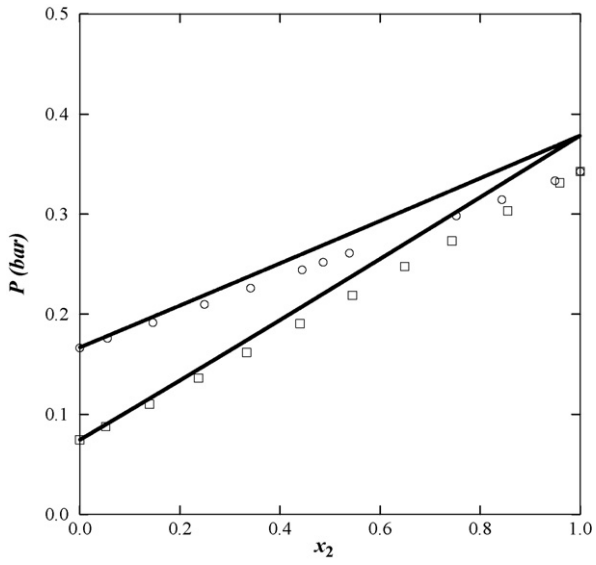

Fig. 6. Predicted constant-temperature *Px* slices (liquid envelope) of propylbenzene (1) + ethylbenzene (2) (circles) and butylbenzene (1) + ethylbenzene (2) (squares) phase diagrams from the GC-SAFT-VR equation compared with experimental data [99] at 373.15 K.

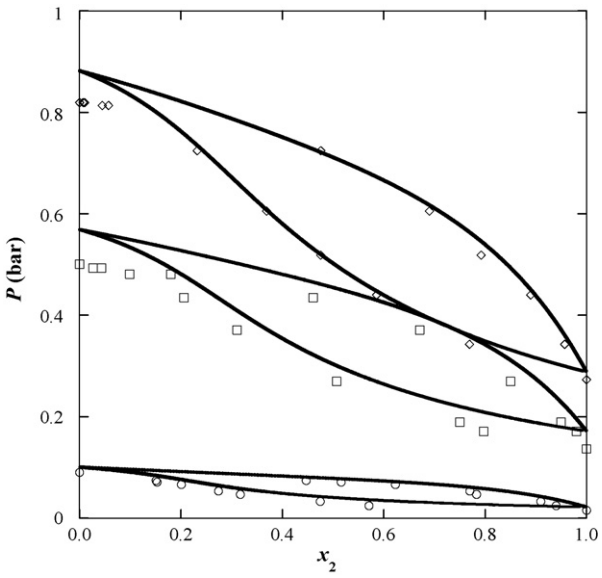

Fig. 8. Predicted constant-temperature *Px* slices of the hexane (1) + 3-pentanone (2) phase diagram from the GC-SAFT-VR equation compared with experimental data [101] at 283.15 K (circles), 325.15 K (squares), and 338.15 K (diamonds).

overpredicted. Results for constant temperature *Px* slices of the propylbenzene + ethylbenzene and butylbenzene + ethylbenzene phase diagrams are compared with experimental data in Fig. 6. Again the theory is able to capture the physical effect of increasing the alkyl chain length on the phase envelope.

We now turn to the vapor–liquid equilibria of *n*-alkane + ketone binary mixtures. The results were obtained using parameters for the CH_3, CH_2, and C=O groups as given in Tables 1–3, without fitting to any binary mixture data. In Fig. 7 we present results for the *n*-heptane + 3-pentanone binary mixture at different temperatures. From the figure we can see that the predicted bubble-dew point curves at these different temperatures, as well as the location of the azeotrope, agrees very well with the experimental data. In contrast, in Fig. 8 we present the binary mixture of *n*-hexane + 3-pentanone at different temperatures, which does not display azeotropic behavior and is also well captured by the theory; simply by decreasing the number of CH_2 groups in the molecular model the GC-SAFT-VR approach is able to accurately predict the significant change in phase behavior. We have also studied binary systems with heavier ketones and in Fig. 9 present results for the *n*-hexane + 3-heptanone system at 338.15 K and in Fig. 10 results for the n-hexane + 3-nonanone system at 333.15, 343.15 and 353.15 K. For both systems good agreement with experimental data is again obtained. We note that the asymmetric ketones, 3-heptanone and 3-nonanone, were not included in the fitting process to determine the intermolecular parameters for the carbonyl group and hence the theoretical predictions presented clearly demonstrate the versatility of the GC-SAFT-VR approach in accurately determining fluid phase behavior.

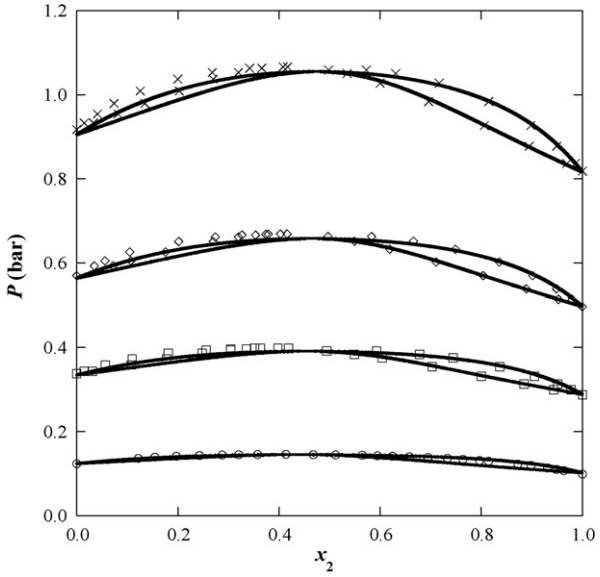

Fig. 7. Predicted constant-temperature *Px* slices of the heptane (1) + 3-pentanone (2) phase diagram from the GC-SAFT-VR equation compared with experimental data [100] at 313.2 K (circles), 338.15 K (squares), 353.15 K (diamonds) and 368.15 K (crosses).

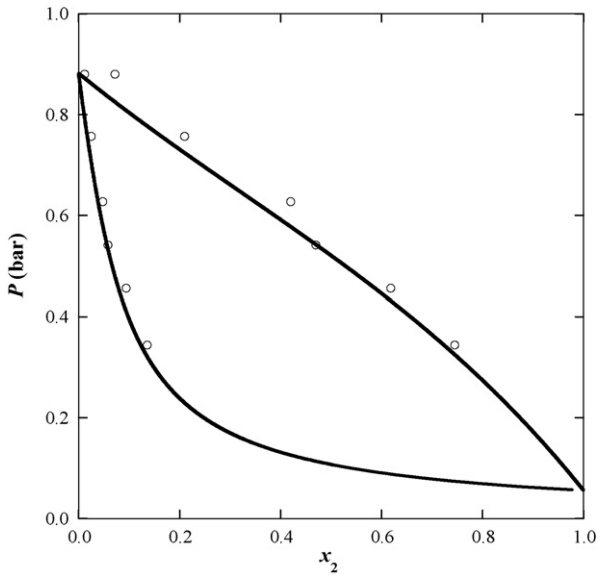

Fig. 9. Predicted constant-temperature *Px* slice of the hexane (1) + 3-heptanone (2) phase diagram from the GC-SAFT-VR equation compared with experimental data [102] at 338.15 K (circles).

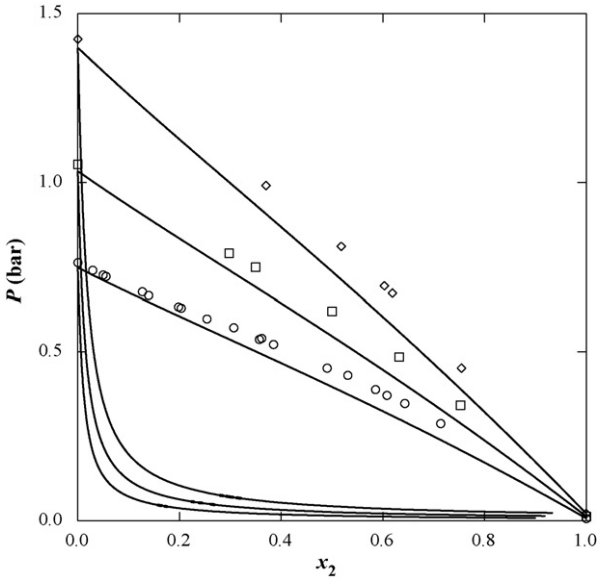

Fig. 10. Predicted constant-temperature *Px* slices of the hexane (1) + 3-nonanone (2) phase diagram from the GC-SAFT-VR equation compared with experimental data [103] at 333.15 K (circles), 343.15 K (squares), and 353.15 K (diamonds).

Finally, in this initial study we have considered the phase diagram of binary mixtures of esters and alkanes and binary mixtures of different esters. The predicted results for these systems are obtained using the group parameters (i.e., CH_2, CH_3, C=O, OCH_2 and OCH_3 groups) determined for pure fluids as given in Tables 1–3. In Fig. 11 we present *Tx* slices of the phase diagram for the binary mixtures of propyl butanoate + *n*-heptane (C_7H_{16}) and propyl butanoate + *n*-nonane (C_9H_{20}) at 1 bar. Although these two systems differ only in the length of the *n*-alkane chain their phase diagrams are quite different: the propyl butanoate + *n*-nonane system displays a positive azeotrope while the mixture of propyl butanoate + *n*-heptane does not show azeotropic behavior. As can be seen from the figure, the theory is able to predict the phase behavior of both systems in excellent agreement with the experimental data without fitting to any binary mixture data,

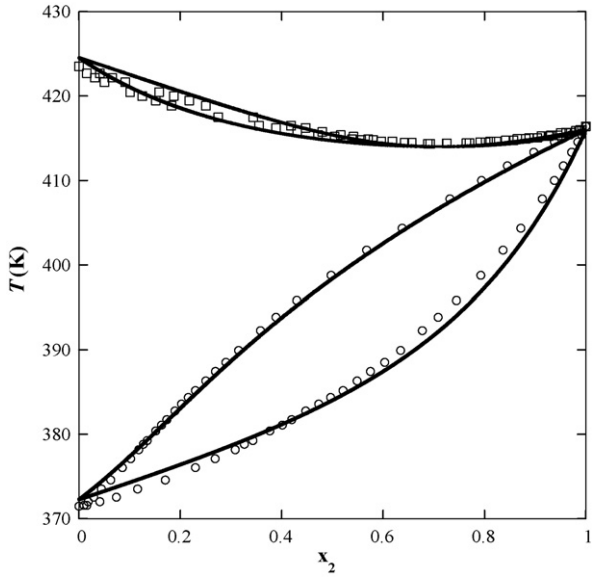

Fig. 11. Predicted constant-pressure *Tx* slices of the *n*-heptane (1) + propyl butanoate (2) (circles) and *n*-octane (1) + propyl butanoate (2) (squares) phase diagrams from the GC-SAFT-VR equation compared with experimental data [104] at 1 bar.

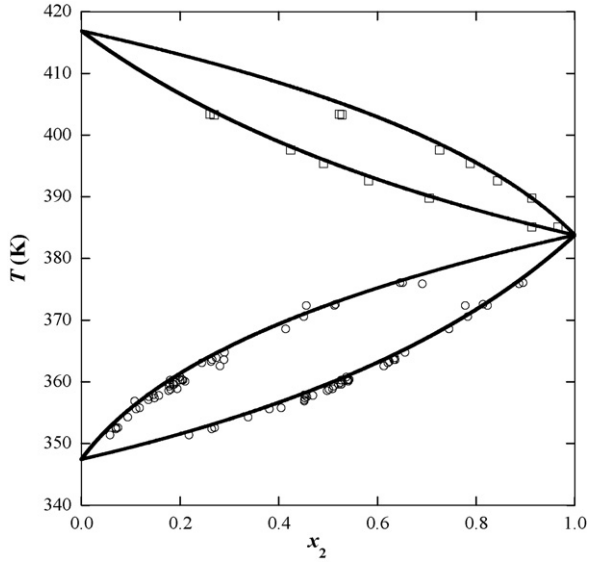

Fig. 12. Predicted constant-pressure *Tx* slice of the methyl hexanoate (1) + methyl octanoate (2) (circles) and methyl decanoate (1) + methyl octanoate (2) (squares) phase diagrams from the GC-SAFT-VR equation compared with experimental data [105] at 0.0667 bar.

i.e., the dramatic change in phase behavior is predicted naturally by the theory when the molecular model for the alkane in increased just two CH_2 groups. Given that all other model parameters remain the same, the physical basis for the azeotrope can be attributed solely to the increased dispersion interactions. We have also considered the phase equilibria of binary mixtures of methyl esters, such as methyl hexanoate + methyl octanoate and methyl decanoate + methyl octanoate as reported in Fig. 12. The GC-SAFT-VR equation again provides an excellent description of the experimental bubble point and dew point curves, given that no parameters have been fitted to any binary mixture data and so the theoretical calculations are pure predictions.

4. Conclusion

In this work, a SAFT-based group-contribution approach developed from the hetero-SAFT-VR equation is proposed. The potential model parameters for a variety of key organic functional groups have been regressed from experimental data for molecules from several different chemical families containing the functional groups of interest. In particular, linear alkanes, branched alkanes, 1-alkenes, alkylbenzenes, ketones, alkyl acetates and methyl esters have been studied in this work to determine transferable parameters for the CH_3, CH_2, CH, CH_2=CH, C_6H_5, C=O, OCH_2 and OCH_3 functional groups. The transferability of these groups was then tested by predicting the phase behavior of heavier molecules within the same chemical family, but not included in the regression process. Good agreement with experimental data is obtained, illustrating that the GC-SAFT-VR approach can accurately predict the phase behavior of pure fluids composed of different functional groups. As a further test of the theory, the model parameters were then used in the study of binary mixtures, where it was shown that the GC-SAFT-VR approach could accurately predict the phase behavior of mixtures containing molecules both included, and not included, in the pure component fitting processes without fitting to any binary mixture data. The binary systems studied were *n*-alkanes, *n*-alkane + ketone, alkylbenzenes, *n*-alkanes + alkylbenzenes, esters, and *n*-alkanes + esters, with the specific systems presented chosen to provide a representative sample of the many possible systems and to highlight the predictive ability of the GC-SAFT-VR approach.

The success of the new approach implies that predictive equations of state can be developed if a truly molecular-based approach is taken, since thermodynamic properties and phase behavior are clearly sensitive to the details of group–group interactions and their placement within a molecule. We also demonstrate that the connectivity of functional groups within a molecule can now be isolated and the physical effects studied. Additionally, through the use of a true group-contribution approach in which a functional group can be added to molecule, while the remaining system parameters do not change, we can isolate the influence of different functional groups on phase behavior. For example, we have shown how the GC-SAFT-VR approach can, by simply increasing the number of CH_2 groups in the molecular model, accurately predict changes in phase behavior as the chain length of one component increases. In this way, in contrast to group-averaging methods, the influence of a single functional group on the thermodynamics and phase behavior of a fluid can be isolated. In future work, the parameters for additional functional groups will be presented, as well as the application of the GC-SAFT-VR approach to polymer systems.

Acknowledgments

We gratefully acknowledge financial support from the National Science Foundation under grant number CTS-0452688 and a Research Experience for Undergraduates Supplement award. The authors would also like to thank Jessica Haley for help with the collection of experimental data used in this study.

Appendix A

In this appendix we present the deviations between the theoretical calculations from GC-SAFT-VR equation and the experimental data [90,91,92] obtained for the different chemical families studied

Table A.1
The average deviation in vapor pressures and saturated liquid densities obtained between experimental data [90] and theoretical results for pure n-alkanes.

n-Alkanes	T (K)	N_{pt}	*AAD P* (%)	*AAD* P^* (%)[a]	T (K)	N_{pt}	*AAD* ρ_{Liq} (%)	*AAD* ρ^*_{Liq} (%)[a]
Correlated								
Propane	130–360	24	13.91	10.35	100–360	27	4.03	2.93
n-Butane	160–420	27	5.72	4.35	140–420	29	3.59	2.81
n-Pentane	180–460	29	4.77	12.06	150–460	32	2.57	2.21
n-Hexane	200–500	31	6.85	16.7	180–500	33	2.48	2.32
n-Heptane	220–560	33	4.52	15.58	190–540	36	3.69	3.17
n-Octane	240–560	33	3.98	15.21	220–560	35	2.7	2.4
n-Nonane	250–590	35	4.2	13.57	220–590	38	2.87	2.41
n-Decane	270–610	35	3.68	12.54	250–610	37	2.68	2.18
n-Dodecane	300–650	36	3.28	9.01	270–650	39	2.64	2.09
n-Hexadecane	350–720	38	5.27	5.88	300–720	43	2.96	2.2
n-Eicosane	390–760	38	7.13	7.01	310–760	46	2.26	1.64
Predicted								
n-Undecane	280–630	36	4.26	12.98	250–630	39	2.5	1.99
n-Tridecane	310–670	37	3.27	9.01	270–670	41	2.76	2.02
n-Tetradecane	320–690	38	3.88	7.67	280–690	42	2.99	2.24
n-Pentadecane	330–700	38	4.09	6.21	290–700	42	2.56	1.87
n-Heptadecane	360–730	38	4.93	5.52	300–730	44	2.59	1.92
n-Octadecane	370–740	38	6.53	6.32	310–740	44	2.6	1.9
n-Nonadecane	380–750	38	7.27	6.53	310–750	45	2.56	1.86
n-Heneicosane	400–770	38	8.64	8.29	320–770	46	2.64	1.9
n-Docosane	410–780	38	10.93	10.46	320–780	47	2.75	1.98
n-Tricosane	410–790	39	9.58	8.8	330–790	47	2.82	2.03
n-Tetracosane	410–800	39	10.55	10.06	330–800	48	2.92	2.12
n-Pentacosane	430–810	39	11.49	11.73	330–810	49	3.2	2.39
n-Hexacosane	440–810	38	11.47	10.96	330–810	49	2.65	1.83
n-Heptacosane	450–820	38	9.97	10.74	340–820	49	2.91	2.07
n-Octacosane	450–830	39	14.02	14.28	340–830	50	3.11	2.27
n-Nonacosane	460–830	38	15.8	15.87	340–830	50	2.82	1.96
n-Triacontane	470–840	38	16.75	19.28	340–840	51	3.25	2.36
n-Dotriacontane	480–850	38	20.11	22.93	350–850	51	3.1	2.22
n-Hexatriacontane	500–870	38	24.26	26.78	350–870	53	3.08	2.27

[a] Obtained using the same set of experimental data as the GC-SAFT-VR approach and modeling the chain as homonuclear with parameters correlated with molecular weight [20].

Table A.2
The average deviation in vapor pressures and saturated liquid densities obtained between experimental data [90] and theoretical results for pure branched alkanes.

Branched alkanes	T (K)	N_{pt}	*AAD P* (%)	T (K)	N_{pt}	*AAD* ρ_{Liq} (%)
Correlated						
4-Methylheptane	230–560	34	4.82	160–560	41	3.16
4-Methyloctane	240–585	36	5.79	160–585	44	3.31
5-Methylnonane	260–610	36	7.65	190–610	43	4.28
3-Ethylpentane	210–540	34	15.8	150–540	40	3.91
3-Ethylhexane	280–565	30	2.69	280–565	30	4.97
3-Ethylheptane	240–590	36	1.99	160–590	44	4.12
Predicted						
2-Methyl heptane	225–550	33	9.83	170–550	39	3.02
2,4-Dimethylhexane	275–550	29	14.49	275–550	29	5.98
2,6-Dimethylheptane	245–575	34	19.08	175–575	41	4.35
2,7-Dimethyloctane	260–600	35	18.09	220–600	39	4.42
Squalane	440–760	43	43.25	270–760	63	2.55

Table A.3
The average deviation in vapor pressures and saturated liquid densities obtained between experimental data [90] and theoretical results for pure 1-alkenes.

Alkenes	T (K)	N_{pt}	$AAD\ P$ (%)	T (K)	N_{pt}	$AAD\ \rho_{Liq}$ (%)
Correlated						
Propene	130–360	24	7.27	90–360	28	2.56
1-Butene	150–415	28	4.71	90–415	34	3.44
1-Pentene	170–460	30	3.9	110–460	36	2.79
1-Hexene	195–495	31	1.71	135–495	37	2.29
1-Heptene	215–535	36	3.64	155–535	39	2.5
1-Octene	235–565	34	3.05	175–565	40	2.34
1-Nonene	245–590	36	4.4	195–590	41	2.26
1-Decene	260–615	37	3.51	210–615	42	2.63
Predicted						
1-Undecene	285–635	36	4.23	225–635	42	2.33
1-Dodecene	290–655	38	4.52	240–655	43	2.48
1-Tridecene	305–675	38	4.14	255–675	43	3.55
1-Tetradecene	315–690	39	4.53	265–690	44	2.85
1-Pentadecene	330–705	39	5.58	270–705	45	2.88
1-Hexadecene	340–720	40	6.19	280–720	46	3.31
1-Heptadecene	355–735	41	7.42	285–735	48	3.56
1-Octadecene	365–745	39	7.45	295–745	46	2.66
1-Nonadecene	380–760	39	7.26	300–760	47	3.75
1-Eicosene	385–770	40	7.32	305–770	48	3.28

Table A.4
The average deviation in vapor pressures and saturated liquid densities obtained between experimental data [90] and theoretical results for pure alkylbenzenes.

Alkylbenzene	T (K)	N_{pt}	$AAD\ P$ (%)	T (K)	N_{pt}	$AAD\ \rho_{Liq}$ (%)
Correlated						
Methylbenzene	220–590	38	10.07	180–590	42	4.9
Ethylbenzene	240–615	39	8.55	180–615	45	4.91
Propylbenzene	255–635	39	2.39	175–635	47	4.14
Butylbenzene	265–660	41	1.99	185–660	49	4.37
Pentylbenzene	290–675	40	2.01	200–675	49	3.99
Hexylbenzene	295–695	41	2.4	215–695	49	3.56
Heptylbenzene	310–710	41	4.91	230–710	49	3.03
Octylbenzene	320–725	42	4.46	240–725	50	3.04
Nonylbenzene	340–740	41	4.33	250–740	50	2.99
Decylbenzene	350–750	41	5.89	260–750	50	2.67
Predicted						
Undecylbenzene	360–760	41	7.31	270–760	50	2.46
Dodecylbenzene	370–780	42	8.84	280–780	51	2.93
Tridecylbenzene	385–790	42	9.44	285–790	52	3.02
Tetradecylbenzene	390–800	42	12.48	290–800	52	2.74
Pentadecylbenzene	400–805	42	13.64	300–805	52	2.17
Hexadecylbenzene	405–815	43	14.36	305–815	53	2.27
Heptadecylbenzene	415–825	42	18.07	295–825	54	2.89
Octadecylbenzene	420–830	42	20.07	310–830	53	3.06

(Tables A.1–A.7). The deviation is expressed as the percentage average absolute deviation for the vapor pressure (*%AAD P*) and saturated liquid density (*%AAD* ρ_{Liq}) obtained from the following expressions, respectively:

$$\%AAD\ P = \frac{1}{N_{pt}} \sum_{i=1}^{N_{pt}} \left| \frac{P_i^{theo} - P_i^{exp}}{P_i^{exp}} \right| \times 100\% \tag{A.1}$$

$$\%AAD\ \rho_{Liq} = \frac{1}{N_{pt}} \sum_{i=1}^{N_{pt}} \left| \frac{\rho_{Liq_i}^{theo} - \rho_{Liq_i}^{exp}}{\rho_{Liq_i}^{exp}} \right| \times 100\% \tag{A.2}$$

where N_{pt} is the number of experimental points, P_i^{exp} and P_i^{theo} are the experimental and calculated value of the vapor pressure; and $\rho_{Liq_i}^{exp}$ and $\rho_{Liq_i}^{theo}$ are the experimental and calculated value of the saturated liquid density, respectively.

Table A.5
The average deviation in vapor pressures and saturated liquid densities obtained between experimental data [90,91] and theoretical results for pure ketones.

Ketones	T (K)	N_{pt}	$AAD\ P$ (%)	T (K)	N_{pt}	$AAD\ \rho_{Liq}$ (%)
Correlated						
3-Pentanone	240–560	33	3.04	240–560	33	2.75
3-Hexanone	240–580	35	5.57	220–580	37	1.38
4-Heptanone	250–600	36	7.21	250–600	36	1.06
4-Octanone	290–615	36	7.77	250–615	38	0.56
5-Nonanone	280–640	37	5.18	270–640	38	2.1
Predicted						
6-Undecanone	298–531	45	4.22	293–358	13	0.95
8-Pentadecanone	443–600	25	4.08	312–351	7	0.84
16-Hentriacontanone				363–573	45	2.16

Table A.6
The average deviation in vapor pressures and saturated liquid densities between experimental data [90] and theoretical results for pure alkyl acetates.

Alkyl acetate	T (K)	N_{pt}	$AAD\ P$ (%)	T (K)	N_{pt}	$AAD\ \rho_{Liq}$ (%)
Correlated						
Propyl acetate	230–540	32	12.54	190–540	36	2.55
Butyl acetate	245–565	33	6.71	205–565	37	2.19
Pentyl acetate	260–580	34	5.76	210–580	38	1.52
Hexyl acetate	280–610	34	3.62	200–610	42	2.08
Heptyl acetate	290–630	35	7.84	240–630	40	2.37
Octyl acetate	300–640	35	6.21	240–640	41	1.97
Nonyl acetate	330–650	33	5.65	260–650	40	2.87
Predicted						
Ethyl butanoate	185–565	39	12.92	185–565	39	1.28
Butyl pentanoate	190–620	44	10.32	190–620	44	1.42
Butyl nonanoate	240–670	44	37.46	240–670	44	1.89
Diethyl succinate	260–660	41	19.46	260–660	41	1.8

Table A.7
The average deviation in vapor pressures and saturated liquid densities between experimental data [90,92] and theoretical results for pure methyl esters.

Methyl ester	T (K)	N_{pt}	$AAD\ P$ (%)	T (K)	N_{pt}	$AAD\ \rho_{Liq}$ (%)
Correlated						
Methyl ethanoate	180–500	33	11.2	180–500	33	2.37
Methyl propanoate	190–520	34	10.42	190–520	34	3.09
Methyl butanoate	190–540	36	5.16	190–540	36	2.26
Methyl pentanoate	298–403	22	2.93	298–403	22	0.29
Methyl hexanoate	287–360	10	4.38	287–360	10	0.32
Methyl heptanoate	333–403	15	0.93	333–403	15	0.46
Methyl octanoate	370–420	11	1.28	284–360	10	0.38
Methyl decanoate	260–660	33	7.65	260–660	33	1.1

References

[1] R. Agrawal, AIChE J. 47 (2001) 967–971.
[2] S.J. Chen, M. Banaszak, M. Radosz, Macromolecules 28 (1995) 1812–1817.
[3] Z. Shen, M.A. McHugh, J. Xu, J. Belardi, S. Kilic, A. Mesiano, S. Bane, C. Karnikas, E. Beckman, R. Enick, Polymer 44 (2003) 1491–1498.
[4] W.G. Chapman, G. Jackson, K.E. Gubbins, Mol. Phys. 65 (1988) 1057–1079.
[5] W.G. Chapman, K.E. Gubbins, G. Jackson, M. Radosz, Ind. Eng. Chem. Res. 29 (1990) 1709–1721.
[6] M.S. Wertheim, J. Stat. Phys. 35 (1984) 19–34.
[7] M.S. Wertheim, J. Stat. Phys. 35 (1984) 35–47.
[8] M.S. Wertheim, J. Stat. Phys. 42 (1986) 459–476.
[9] M.S. Wertheim, J. Stat. Phys. 42 (1986) 477–492.
[10] I.G. Economou, Ind. Eng. Chem. Res. 41 (2002) 953–962.
[11] E.A. Müller, K.E. Gubbins, Ind. Eng. Chem. Res. 40 (2001) 2193–2211.
[12] A. Gil-Villegas, A. Galindo, P.J. Whitehead, S.J. Mills, G. Jackson, A.N. Burgess, J. Chem. Phys. 106 (1997) 4168–4186.
[13] A. Galindo, L.A. Davies, A. Gil-Villegas, G. Jackson, Mol. Phys. 93 (1998) 241–252.
[14] C. McCabe, A. Galindo, A. Gil-Villegas, G. Jackson, Int. J. Thermophys. 19 (1998) 1511–1522.
[15] C. McCabe, A. Gil-Villegas, G. Jackson, J. Phys. Chem. B 102 (1998) 4183–4188.
[16] C. McCabe, G. Jackson, Phys. Chem. Chem. Phys. 1 (1999) 2057–2064.
[17] C. McCabe, A. Galindo, M.N. Garcia-Lisbona, G. Jackson, Ind. Eng. Chem. Res. 40 (2001) 3835–3842.
[18] C. McCabe, S.B. Kiselev, Fluid Phase Equilib. 219 (2004) 3–9.
[19] C. McCabe, S.B. Kiselev, Ind. Eng. Chem. Res. 43 (2004) 2839–2851.
[20] P. Paricaud, A. Galindo, G. Jackson, Ind. Eng. Chem. Res. 43 (2004) 6871–6889.
[21] A. Galindo, L.J. Florusse, C.J. Peters, Fluid Phase Equilib. 160 (1999) 123–131.
[22] E.J.M. Filipe, E. de Azevedo, L.F.G. Martins, V.A.M. Soares, J.C.G. Calado, C. McCabe, G. Jackson, J. Phys. Chem. B 104 (2000) 1315–1321.
[23] E.J.M. Filipe, L.F.G. Martins, J.C.G. Calado, C. McCabe, G. Jackson, J. Phys. Chem. B 104 (2000) 1322–1325.
[24] C. McCabe, L.M.B. Dias, G. Jackson, E.J.M. Filipe, Phys. Chem. Chem. Phys. 3 (2001) 2852–2855.
[25] L.X. Sun, H.G. Zhao, S.B. Kiselev, C. McCabe, Fluid Phase Equilib. 228 (2005) 275–282.
[26] L.X. Sun, H.G. Zhao, S.B. Kiselev, C. McCabe, J. Phys. Chem. B 109 (2005) 9047–9058.
[27] H.G. Zhao, P. Morgado, C. McCabe, A. Gil-Villegas, J. Phys. Chem. B 110 (2006) 24083.
[28] L. Sun, H. Zhao, C. McCabe, AIChE J. 53 (2007) 720–731.
[29] C. McCabe, A. Galindo, A. Gil-Villegas, G. Jackson, J. Phys. Chem. B 102 (1998) 8060–8069.
[30] R.P. Bonifacio, E.J.M. Filipe, C. McCabe, M.F.C. Gomes, A.A.H. Padua, Mol. Phys. 100 (2002) 2547–2553.
[31] P. Morgado, C. McCabe, E.J.M. Filipe, Fluid Phase Equilib. 228 (2005) 389–393.
[32] P. Morgado, H. Zhao, F.J. Blas, C. McCabe, L.P.N. Rebelo, E.J.M. Filipe, J. Phys. Chem. B 111 (2007) 2856–2863.
[33] A. Galindo, S.J. Burton, G. Jackson, D.P. Visco, D.A. Kofke, Mol. Phys. 100 (2002) 2241–2259.
[34] L.M.B. Dias, R.P. Bonifacio, E.J.M. Filipe, J.C.G. Calado, C. McCabe, G. Jackson, Fluid Phase Equilib. 205 (2003) 163–170.
[35] L.M.B. Dias, E.J.M. Filipe, C. McCabe, T. Cordeiro, J.C.G. Calado, J. Phys. Chem. B 111 (2007) 5284–5289.
[36] A. Galindo, A. Gil-Villegas, P.J. Whitehead, G. Jackson, A.N. Burgess, J. Phys. Chem. B 102 (1998) 7632–7639.
[37] M.C. dos Ramos, F.J. Blas, Mol. Phys. 105 (2007) 1319–1334.
[38] C. McCabe, A. Galindo, P.T. Cummings, J. Phys. Chem. B 107 (2003) 12307–12314.
[39] G.N.I. Clark, A.J. Haslam, A. Galindo, G. Jackson, Mol. Phys. 104 (2006) 3561–3581.
[40] H.G. Zhao, Y. Ding, C. McCabe, J. Chem. Phys. 127 (2007) 4514.
[41] F.J. Blas, A. Galindo, Fluid Phase Equilib. 194–197 (2002) 501–509.
[42] A. Galindo, F.J. Blas, J. Phys. Chem. B 106 (2002) 4503–4515.
[43] C.M. Colina, A. Galindo, F.J. Blas, K.E. Gubbins, Fluid Phase Equilib. 222 (2004) 77–85.
[44] C.M. Colina, K.E. Gubbins, J. Phys. Chem. B 109 (2005) 2899–2910.
[45] M.C. dos Ramos, F.J. Blas, A. Galindo, Fluid Phase Equilib. 261 (2007) 359–365.
[46] M.C. dos Ramos, F.J. Blas, A. Galindo, J. Phys. Chem. C 111 (2007) 15924–15934.
[47] A. Galindo, A. Gil-Villegas, G. Jackson, A.N. Burgess, J. Phys. Chem. B 103 (1999) 10272–10281.
[48] A. Gil-Villegas, A. Galindo, G. Jackson, Mol. Phys. 99 (2001) 531–546.
[49] B.H. Patel, P. Paricaud, A. Galindo, G.C. Maitland, Ind. Eng. Chem. Res. 42 (2003) 3809–3823.
[50] H.G. Zhao, M.C. dos Ramos, C. McCabe, J. Chem. Phys. 126 (2007) 4503.
[51] H. Adidharma, M. Radosz, Ind. Eng. Chem. Res. 37 (1998) 4453–4462.
[52] C.K. Chen, M. Banaszak, M. Radosz, J. Phys. Chem. B 102 (1998) 2427–2431.
[53] F.J. Blas, L.F. Vega, Ind. Eng. Chem. Res. 37 (1998) 660–674.
[54] G. Sadowski, Fluid Phase Equilib. 149 (1998) 75–89.
[55] J. Jiang, J.M. Prausnitz, J. Chem. Phys. 111 (1999) 5964.
[56] M.L.L. Paredes, R. Nobrega, F.W. Tavares, Ind. Eng. Chem. Res. 40 (2001) 1748–1754.
[57] J.C. Pamies, L.F. Vega, Mol. Phys. 100 (2002) 2519–2529.
[58] S.J. Chen, I.G. Economou, M. Radosz, Macromolecules 25 (1992) 4987–4995.
[59] B.M. Hasch, M.A. McHugh, J. Polym. Sci. B: Polym. Phys. 33 (1995) 715–723.
[60] S.H. Lee, B.M. Hasch, M.A. McHugh, Fluid Phase Equilib. 117 (1996) 61–68.
[61] N. Koak, R.M. Visser, T.W. de Loos, Fluid Phase Equilib. 160 (1999) 835–846.
[62] S. Takishima, M.L. O'Neill, K.P. Johnston, Ind. Eng. Chem. Res. 36 (1997) 2821–2833.
[63] C.J. Gregg, F.P. Stein, M. Radosz, Macromolecules 27 (1994) 4972–4980.
[64] G. Sadowski, L.V. Mokrushina, W. Arlt, Fluid Phase Equilib. 139 (1997) 391–403.
[65] F. Tumakaka, J. Gross, G. Sadowski, Fluid Phase Equilib. 194–197 (2002) 541–551.
[66] M. Lora, F. Rindfleisch, M.A. McHugh, J. Appl. Polym. Sci. 73 (1999) 1979–1991.

[67] C. McCabe, A. Gil-Villegas, G. Jackson, F. Del Rio, Mol. Phys. 97 (1999) 551–558.
[68] Y. Peng, H.G. Zhao, C. McCabe, Mol. Phys. 104 (2006) 571–586.
[69] S. Tamouza, J.P. Passarello, P. Tobaly, J.C. de Hemptinne, Fluid Phase Equilib. 222 (2004) 67–76.
[70] S. Tamouza, J.P. Passarello, P. Tobaly, J.C. de Hemptinne, Fluid Phase Equilib. 228 (2005) 409–419.
[71] T.X.N. Thi, S. Tamouza, P. Tobaly, J.P. Passarello, J.C. de Hemptinne, Fluid Phase Equilib. 238 (2005) 254–261.
[72] C. Le Thi, S. Tamouza, J.P. Passarello, P. Tobaly, J.C. de Hemptinne, Ind. Eng. Chem. Res. 45 (2006) 6803–6810.
[73] A. Tihic, G.M. Kontogeorgis, N. von Sohns, M.L. Michelsen, L. Constantinou, Ind. Eng. Chem. Res. 47 (2008) 5092–5101.
[74] J. Gross, G. Sadowski, Ind. Eng. Chem. Res. 40 (2001) 1244–1260.
[75] A. Lymperiadis, C.S. Adjiman, A. Galindo, G. Jackson, J. Chem. Phys. 127 (2007) 234903.
[76] P.J. Leonard, D. Henderson, J.A. Barker, Trans. Faraday Soc. 66 (1970) 2439–2452.
[77] T. Boublik, J. Chem. Phys. 53 (1970) 471–472.
[78] G.A. Mansoori, N.F. Carnahan, K.E. Starling, T.W. Leland, J. Chem. Phys. 54 (1971) 1523–1525.
[79] N.F. Carnahan, K.E. Starling, J. Chem. Phys. 51 (1969) 635–636.
[80] B.H. Patel, H. Docherty, S. Varga, A. Galindo, G.C. Maitland, Mol. Phys. 103 (2005) 129–139.
[81] S. Kirkpatrick, C.D. Gelatt, M.P. Vecchi, Science 220 (1983) 671–680.
[82] W.B. Dolan, P.T. Cummings, M.D. Levan, AIChE J. 35 (1989) 725–736.
[83] G. Jackson, K.E. Gubbins, Pure Appl. Chem. 61 (1989) 1021–1026.
[84] A.L. Archer, M.D. Amos, G. Jackson, I.A. McLure, Int. J. Thermophys. 17 (1996) 201–211.
[85] T. Lafitte, D. Bessieres, M.M. Pineiro, J.L. Daridon, J. Chem. Phys. 124 (2006) 024509.
[86] J. Sponer, J. Leszczynski, P. Hobza, Biopolymers 61 (2001) 3–31.
[87] D. NguyenHuynh, J.P. Passarello, P. Tobaly, J.C. de Hemptinne, Fluid Phase Equilib. 264 (2008) 62–75.
[88] H.G. Zhao, C. McCabe, J. Chem. Phys. 125 (2006).
[89] NIST Chemistry Webbook, 1991.
[90] DIPPR 801 Tables, Thermophysical Properties Database, 2005.
[91] B.D. Smith, R. Srivastava, Thermodynamic Data for Pure Compounds. Part A. Hydrocarbons and Ketones, Elsevier, London, 1986.
[92] U. Westhaus, T. Droge, R. Sass, Fluid Phase Equilib. 158 (1999) 429–435.
[93] J. Wisniak, E. Magen, M. Shachar, I. Zeroni, R. Reich, H. Segura, J. Chem. Eng. Data 42 (1997) 458–462.
[94] D.S. Jan, H.Y. Shiau, F.N. Tsai, J. Chem. Eng. Data 39 (1994) 438–440.
[95] M.L. McGlashan, A.G. Williamson, Trans. Faraday Soc. 57 (1961) 588–600.
[96] P.C. Joyce, M.C. Thies, J. Chem. Eng. Data 43 (1998) 819–822.
[97] C.P. Yang, M. van Winkle, Int. Chem. Eng. 47 (1955) 293–296.
[98] H.S. Myers, Ind. Eng. Chem. 47 (1955) 2215–2219.
[99] B. Wisniewska, J. Chem. Thermodyn. 19 (1987) 897–901.
[100] G. Geiseler, H. Kohler, Ber. Bunsen-Ges. Phys. Chem. 72 (1968) 697–706.
[101] R. Barraza, S. Diaz, J. Edwards, P. Tapia, Z. Phys. Chem. 117 (1979) 43–54.
[102] V.C. Maripuri, G.A. Ratcliff, J. Appl. Chem. Biotechnol. 22 (1972) 899.
[103] H. Renon, J.M. Prausnitz, Ind. Eng. Chem. Process Des. Dev. 7 (1968) 220–225.
[104] J. Ortega, C. Gonzalez, S. Galvan, J. Chem. Eng. Data 46 (2001) 904–912.
[105] A. Rose, W.R. Supina, J. Chem. Eng. Data 6 (1961) 173–179.